Equivalence of knife-edge diffraction model and uniform geometrical theory of diffraction applying Fresnel approximation for an absorbing screen

X. Du and J. Takada

The knife-edge diffraction model (KED) and the uniform geometrical theory of diffraction (UTD) have been widely used to predict the shadowing effect at millimetre-wave (mmWave) bands. This letter proposes a mathematical derivation to rigorously prove that, for an absorbing screen, UTD applying the narrow-angle Fresnel approximation is equivalent to KED. The simulation scenarios are designed to validate the proposal by comparing KED with UTD in the narrow-angle (less than 20°) and wide-angle (over 20°) regions at mmWave bands (20 GHz - 100 GHz). Simulated results agree with the proposal that KED is identical to UTD with a low error of less than 0.1 dB in the narrow-angle region, while they have a difference with an error of over 1 dB in the wide-angle region. In addition, the average computational time is measured and results in both UTD and KED taking approximately 8.0 ms for one test. From the proposal, it can be theoretically explained the differences and similarities between KED and UTD for an absorbing screen.

Introduction: The prediction method of the forward scattering can be utilized to quantify the shadowing effect in the 5$^{\text{th}}$ generation (5G) mobile communication systems at the millimetre-wave (mmWave) bands [1, 2, 3]. To predict the shadowing gain accurately and quickly, the knife-edge diffraction model (KED) [4] and the uniform geometrical theory of diffraction (UTD) [5, 6] have been developed and widely used. KED based on physical optics (PO) is the analytical solution of the Kirchhoff approximation (KA) by using the Fresnel approximation [7]. Since KED models the obstacle as an absorbing half plane, it does not concern boundary conditions, i.e., polarization and surface impedance. On the other hand, UTD based on geometrical optics (GO) is a closed-form solution approximated by the exact solution of the canonical problem asymptotically [8, 9, 10]. Although UTD can deal with boundary conditions, the diffraction coefficient of UTD for an absorbing screen does not need to consider polarization [11].

The comparison between ray-based UTD and KED has been studied by several previous works. The work in [12] compared the ray tracking technique with KED in an urban environment, and it found that the ray-based method outperformed KED in accuracy for the wide-angle region. In the work [13], KED and UTD were simulated by comparing them with the measurement results, and it concluded that UTD had a significant improvement in accuracy with the wide-angle incidence or diffraction. However, those works only compared them by using numerical simulation or measurement, which did not provide further mathematical investigations to theoretically explain the differences and similarities between KED and UTD. This work aims to connect KED and UTD through rigorous mathematical approaches. In this letter, the authors propose a detailed derivation to rigorously prove that, for an absorbing screen, UTD applying the narrow-angle Fresnel approximation is equivalent to KED.

Proposed approaches to connect KED and UTD: Figures 1(a) and 1(b) show the cross-section view of the model in the shadowed and lit regions, respectively. A semi-infinite-height absorbing screen is placed between the transmitter (Tx) and the receiver (Rx). The parameters l_{i} and l_{d} denote the distances from the diffraction point to the Tx and Rx. The parameters ϕ_{i} and ϕ_{d} denote the angles of the incident and diffracted rays, respectively, measured in a plane perpendicular to the edge at the diffraction point. The parameters d_1 and d_2 are the distances perpendicular to the screen from the diffraction point to the Tx and Rx.

The original KED assumes that the screen is normal to the Tx-Rx line [4], as shown in Fig. 1. The parameters h and $-h$ are the distances parallel to the screen from the diffraction point to the Tx-Rx line in the shadowed and lit regions, respectively. The total electric field calculated by KED is formulated in [4] as

$$E^{\text{KED}} = j\frac{E_{\text{i}}e^{-j\pi/4}}{\sqrt{2}}\int_{\nu}^{\infty} e^{-j(\pi/2)X^2}\mathrm{d}X \tag{1}$$

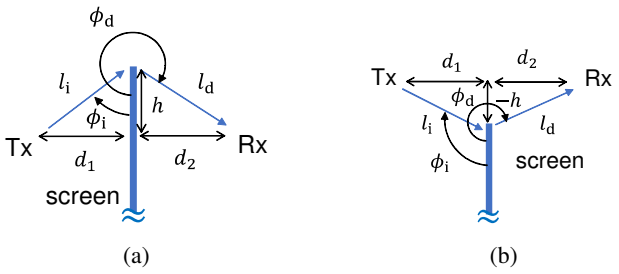

Fig. 1 *Location of screen the antennas (cross-section view). (a) model in the shadowed region, (b) model in the lit region*

with

$$E_{\text{i}} = \frac{\lambda E_0 e^{-jk_0(d_1+d_2)}}{4\pi(d_1+d_2)} \quad , \quad \nu = h\sqrt{\frac{2}{\lambda}\left(\frac{1}{d_1}+\frac{1}{d_2}\right)} \tag{2}$$

where j, E_{i}, E_0, ν, λ, and k_0 are the imaginary unit, the scalar electric field of the spherical wave incident to the Rx, the scalar electric field of the source (Tx), Fresnel-Kirchhoff parameter, wavelength, and wave number in the free space, respectively.

On the other hand, since this work focuses on the comparison of UTD with the forward scattering KED, the reflected field for the backward scattering is not considered in the UTD calculation. UTD for an absorbing screen with a spherical wave incidence explained in [11] calculates the total electric field as

$$E^{\text{UTD}} = \begin{cases} E_{\text{d}} & \text{(for shadowed region)} \\ E_{\text{i}} + E_{\text{d}} & \text{(for lit region)} \end{cases} , \tag{3}$$

with

$$E_{\text{d}} = -\frac{\lambda E_0 e^{-j(k_0 l_{\text{i}}+\frac{\pi}{4})}}{8\pi l_{\text{i}}\sqrt{2\pi k_0}}\sec\frac{\phi_{\text{d}}-\phi_{\text{i}}}{2}F(t)\sqrt{\frac{l_{\text{i}}}{l_{\text{d}}(l_{\text{i}}+l_{\text{d}})}}e^{-jk_0 l_{\text{d}}} \tag{4}$$

where E_{d} and $F(t)$ denote the diffracted scalar electric field and the modified Fresnel integral defined by (5), respectively.

$$F(t) = j2\sqrt{t}e^{jt}\int_{\sqrt{t}}^{\infty} e^{-j\tau^2}\mathrm{d}\tau \quad , \quad t = 2k_0\frac{l_{\text{i}}l_{\text{d}}}{l_{\text{i}}+l_{\text{d}}}\cos^2\frac{\phi_{\text{d}}-\phi_{\text{i}}}{2}. \tag{5}$$

To connect KED and UTD, specifically, by letting $\tau = \sqrt{\pi/2}X$, the integral in (5) now reads

$$\int_{\sqrt{t}}^{\infty} e^{-j\tau^2}\mathrm{d}\tau = \sqrt{\frac{\pi}{2}}\int_{\sqrt{\frac{4k_0}{\pi}\frac{l_{\text{i}}l_{\text{d}}}{l_{\text{i}}+l_{\text{d}}}\cos^2\frac{\phi_{\text{d}}-\phi_{\text{i}}}{2}}}^{\infty} e^{-j(\pi/2)X^2}\mathrm{d}X. \tag{6}$$

Note that

$$\frac{4k_0}{\pi}\frac{l_{\text{i}}l_{\text{d}}}{l_{\text{i}}+l_{\text{d}}}\cos^2\frac{\phi_{\text{d}}-\phi_{\text{i}}}{2} = \frac{2}{\lambda}\frac{2l_{\text{i}}l_{\text{d}}}{l_{\text{i}}+l_{\text{d}}}\left(1+\cos(\phi_{\text{d}}-\phi_{\text{i}})\right), \tag{7}$$

and apply the law of cosine as

$$2l_{\text{i}}l_{\text{d}}\cos(\phi_{\text{d}}-\phi_{\text{i}}) = l_{\text{i}}^2 + l_{\text{d}}^2 - (d_1+d_2)^2, \tag{8}$$

then (7) becomes

$$\frac{2}{\lambda}\frac{2l_{\text{i}}l_{\text{d}}}{l_{\text{i}}+l_{\text{d}}}\left(1+\cos(\phi_{\text{d}}-\phi_{\text{i}})\right) = \frac{2}{\lambda}\frac{(l_{\text{i}}+l_{\text{d}})^2-(d_1+d_2)^2}{l_{\text{i}}+l_{\text{d}}}. \tag{9}$$

Here, the Fresnel approximation [14, 15] for $l_{\text{i,d}}$ is applied as

$$l_{\text{i,d}} \approx \begin{cases} d_{1,2} + \dfrac{h^2}{2d_{1,2}} & \text{(for phase variations)} \\ d_{1,2} & \text{(for amplitude variations)} \end{cases} \tag{10}$$

given that the narrow-angle condition of the Fresnel approximation is held, i.e., $|\arctan(h/d_2)| \le 20^\circ$ [16]. Accordingly, (9) can be approximated as

$$\frac{2}{\lambda}\frac{2l_{\text{i}}l_{\text{d}}}{l_{\text{i}}+l_{\text{d}}}\left(1+\cos(\phi_{\text{d}}-\phi_{\text{i}})\right) \approx h^2\frac{2}{\lambda}\left(\frac{1}{d_1}+\frac{1}{d_2}\right) = \nu^2 \tag{11}$$

according to (2). By substituting (7) and (11) into (6), the Fresnel integral becomes

$$\int_{\sqrt{t}}^{\infty} e^{-j\tau^2}\mathrm{d}\tau = \sqrt{\frac{\pi}{2}}\int_{|\nu|}^{\infty} e^{-j(\pi/2)X^2}\mathrm{d}X. \tag{12}$$

Through substituting (5), and (12) into (4), the diffracted field becomes

$$E_{\mathrm{d}} \approx \frac{\lambda E_0 e^{-jk_0 l_{\mathrm{i}}}}{4\pi l_{\mathrm{i}}} \sqrt{\frac{l_{\mathrm{i}}}{l_{\mathrm{d}}(l_{\mathrm{i}}+l_{\mathrm{d}})}} e^{-jk_0 l_{\mathrm{d}}} \frac{-e^{-j\frac{\pi}{4}}}{2\sqrt{2\pi k_0}} \times j2\sqrt{2k_0 \frac{l_{\mathrm{i}} l_{\mathrm{d}}}{l_{\mathrm{i}}+l_{\mathrm{d}}}} \left|\cos\frac{\phi_{\mathrm{d}}-\phi_{\mathrm{i}}}{2}\right| e^{j2k_0 \frac{l_{\mathrm{i}} l_{\mathrm{d}}}{l_{\mathrm{i}}+l_{\mathrm{d}}} \cos^2\frac{\phi_{\mathrm{d}}-\phi_{\mathrm{i}}}{2}} \times \sec\frac{\phi_{\mathrm{d}}-\phi_{\mathrm{i}}}{2} \sqrt{\frac{\pi}{2}} \int_{|\nu|}^{\infty} e^{-j(\pi/2)X^2} \mathrm{d}X. \quad (13)$$

According to the similar approaches with (9) and (10), the exponential terms of (13) can be approximated as

$$e^{-jk_0 l_{\mathrm{i}}} e^{-jk_0 l_{\mathrm{d}}} e^{j2k_0 \frac{l_{\mathrm{i}} l_{\mathrm{d}}}{l_{\mathrm{i}}+l_{\mathrm{d}}} \cos^2\frac{\phi_{\mathrm{d}}-\phi_{\mathrm{i}}}{2}} \approx e^{-jk_0(d_1+d_2)}. \quad (14)$$

By substituting (14) into (13), we have

$$E_{\mathrm{d}} \approx \frac{-je^{-j\frac{\pi}{4}}}{\sqrt{2}} \frac{\lambda E_0 e^{-jk_0(d_1+d_2)}}{4\pi(l_{\mathrm{i}}+l_{\mathrm{d}})} \sec\frac{\phi_{\mathrm{d}}-\phi_{\mathrm{i}}}{2} \left|\cos\frac{\phi_{\mathrm{d}}-\phi_{\mathrm{i}}}{2}\right| \times \int_{|\nu|}^{\infty} e^{-j(\pi/2)X^2} \mathrm{d}X. \quad (15)$$

Here, the denominator $l_{\mathrm{i,d}}$ can be approximated as $d_{1,2}$ according to (10). Through substituting (2) into (15), the diffracted field is expressed as

$$E_{\mathrm{d}} \approx -j\frac{E_{\mathrm{i}} e^{-j\frac{\pi}{4}}}{\sqrt{2}} \sec\frac{\phi_{\mathrm{d}}-\phi_{\mathrm{i}}}{2} \left|\cos\frac{\phi_{\mathrm{d}}-\phi_{\mathrm{i}}}{2}\right| \int_{|\nu|}^{\infty} e^{-j(\pi/2)X^2} \mathrm{d}X. \quad (16)$$

In the shadowed region, due to $\phi_{\mathrm{d}} - \phi_{\mathrm{i}} > \pi$ and $\nu > 0$, we have

$$\sec\frac{\phi_{\mathrm{d}}-\phi_{\mathrm{i}}}{2} \left|\cos\frac{\phi_{\mathrm{d}}-\phi_{\mathrm{i}}}{2}\right| = -1 \ , \ |\nu| = \nu. \quad (17)$$

Accordingly, (15) now reads

$$E_{\mathrm{d}} \approx j\frac{E_{\mathrm{i}} e^{-j\frac{\pi}{4}}}{\sqrt{2}} \int_{\nu}^{\infty} e^{-j(\pi/2)X^2} \mathrm{d}X. \quad (18)$$

The total field calculated by UTD in the shadowed region is considered as the diffracted field alone, and the result is identical to KED in (1) as

$$E^{\mathrm{UTD}}\big|_{\nu>0} = E_{\mathrm{d}} \approx j\frac{E_{\mathrm{i}} e^{-j\frac{\pi}{4}}}{\sqrt{2}} \int_{\nu}^{\infty} e^{-j(\pi/2)X^2} \mathrm{d}X = E^{\mathrm{KED}}\big|_{\nu>0}. \quad (19)$$

In the lit region, due to $\phi_{\mathrm{d}} - \phi_{\mathrm{i}} < \pi$ and $\nu < 0$, we have

$$\sec\frac{\phi_{\mathrm{d}}-\phi_{\mathrm{i}}}{2} \left|\cos\frac{\phi_{\mathrm{d}}-\phi_{\mathrm{i}}}{2}\right| = 1 \ , \ |\nu| = -\nu. \quad (20)$$

Therefore, (15) reduces to

$$E_{\mathrm{d}} \approx -j\frac{E_{\mathrm{i}} e^{-j\frac{\pi}{4}}}{\sqrt{2}} \int_{-\nu}^{\infty} e^{-j(\pi/2)X^2} \mathrm{d}X. \quad (21)$$

Note that

$$\int_{-\nu}^{\infty} e^{-j(\pi/2)X^2} \mathrm{d}X = \sqrt{2}e^{-j\frac{\pi}{4}} - \int_{\nu}^{\infty} e^{-j(\pi/2)X^2} \mathrm{d}X. \quad (22)$$

Consequently, (21) becomes

$$E_{\mathrm{d}} \approx -E_{\mathrm{i}} + j\frac{E_{\mathrm{i}} e^{-j\frac{\pi}{4}}}{\sqrt{2}} \int_{\nu}^{\infty} e^{-j(\pi/2)X^2} \mathrm{d}X. \quad (23)$$

The total field calculated by UTD in the lit region is considered as the sum of the diffracted and incident fields, and the result is equivalent to KED as

$$E^{\mathrm{UTD}}\big|_{\nu<0} = E_{\mathrm{i}} + E_{\mathrm{d}} \approx j\frac{E_{\mathrm{i}} e^{-j\frac{\pi}{4}}}{\sqrt{2}} \int_{\nu}^{\infty} e^{-j(\pi/2)X^2} \mathrm{d}X = E^{\mathrm{KED}}\big|_{\nu<0}. \quad (24)$$

In the transition region, due to $\phi_{\mathrm{d}} - \phi_{\mathrm{i}} = \pi$ and $\nu = 0$ at the shadow boundary (SB), $\sec\{(\phi_{\mathrm{d}} - \phi_{\mathrm{i}})/2\}$ has the singularity at SB. The value of UTD at SB is defined to be the limiting value as

$$\lim_{\nu\to+0} E^{\mathrm{UTD}} = \lim_{\nu\to-0} E^{\mathrm{UTD}} \approx j\frac{E_{\mathrm{i}} e^{-j\pi/4}}{\sqrt{2}} \int_{0}^{\infty} e^{-j(\pi/2)X^2} \mathrm{d}X \quad (25)$$

according to (19) and (24) for $\nu \to +0$ and $\nu \to -0$, respectively. Thus, UTD at SB has the same value compared with KED as

$$\lim_{\nu\to0} E^{\mathrm{UTD}} \approx j\frac{E_{\mathrm{i}} e^{-j\pi/4}}{\sqrt{2}} \int_{0}^{\infty} e^{-j(\pi/2)X^2} \mathrm{d}X = E^{\mathrm{KED}}\big|_{\nu=0}. \quad (26)$$

Ultimately, from (19), (24), and (26), the UTD for an absorbing screen can be approximated as KED despite the sign of ν. Viz.

$$E^{\mathrm{UTD}} \approx E^{\mathrm{KED}} \quad (27)$$

given that the narrow-angle condition of the Fresnel approximation is held.

Simulation: Due to the lack of the exact solution for an absorbing screen, this work considers UTD as the reference to compare it with KED. Since the original KED cannot deal with the multiple-diffraction problem, three scenarios of the single-diffraction problems are simulated. For the sake of simplicity, a semi-infinite-height absorbing screen, which is uniform along the z-axis, is considered. As shown in Fig. 2(a), scenario 1 varies the distance d_2 from 0.05 m to 10 m with an interval of 0.05 m for the frequencies $f = 20$ GHz, $f = 40$ GHz, $f = 60$ GHz, $f = 80$ GHz, and $f = 100$ GHz, respectively.

Scenario 2 varies the observation angle θ from $-90°$ to $90°$ with an interval of $1°$ at $f = 100$ GHz, as depicted in Fig. 2(b), where θ is defined as the azimuth angle measured from the x-axis, i.e., $\theta = \arctan(-h/d_2)$. Scenarios 1 and 2 assume that a uniform plane wave travelling along the x-axis is a normal incidence on the screen. However, scenarios 1 and 2 do not vary incident angles, while the narrow-angle approximation is also applied at the Tx side in (10).

To investigate the characteristics of angles for both the Tx and Rx, scenario 3 rotates the Tx and Rx with the same angle θ in clockwise and counterclockwise orientations, respectively, as shown in Fig. 2(c). The angle θ is varied from $-90°$ to $90°$ with an interval of $1°$. The Tx uses a point source at $f = 100$ GHz. Since KED requires that the screen is normal to the Tx-Rx line [4], the Tx and Rx are set with the same height, i.e., $l_{\mathrm{i}} \sin\theta = l_{\mathrm{d}} \sin\theta \Rightarrow l_{\mathrm{i}} = l_{\mathrm{d}}$.

Continuous waves (CW) are used in simulations. For an absorbing screen, both KED and UTD do not need to concern polarization [4, 11]. The simulation parameters are summarized in Table 1. The processor of the calculating computer is an Intel(R) Core(TM) i9-12900K CPU @ 3.19 GHz. The usable installed memory of the calculating computer is 63.7 GB. The system type of the calculating computer is a 64-bit operating system with an x64-based processor. The simulation software is MATLAB.

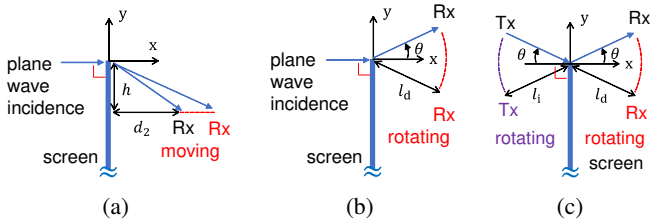

Fig. 2 *Simulation environments (cross-section view). (a) scenario 1, (b) scenario 2, (c) scenario 3*

Table 1: Values of the simulation parameters

Parameters	Scenario 1	Scenario 2	Scenario 3
E_0 (V/m)	1	1	1
f (GHz)	[20, 100]	100	100
h (m)	1	-	-
d_2 (m)	[0.05, 10]	-	-
θ (°)	-	$[-90, 90]$	$[-90, 90]$
l_{d} (m)	-	0.01	0.01
l_{i} (m)	-	-	0.01

Results and Discussions: To evaluate the shadowing gain, the power of the total field normalized by a free-space incident field, i.e., $|E^{\mathrm{KED}}|^2/|E_{\mathrm{i}}|^2$ or $|E^{\mathrm{UTD}}|^2/|E_{\mathrm{i}}|^2$ for KED or UTD, respectively, is calculated on a decibel

(dB) scale. Figures 3(a), 3(b), and 3(c) show the simulated results for scenarios 1, 2, and 3, respectively.

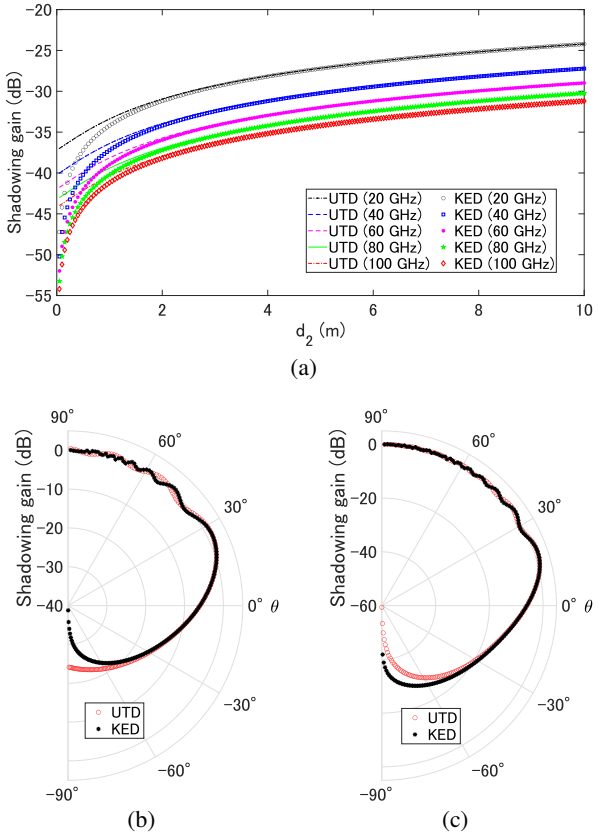

Fig. 3 *Simulated results of the shadowing gain. (a) scenario 1, (b) scenario 2, (c) scenario 3*

The characteristics of distances and frequencies are shown in Fig. 3(a). The average errors between UTD and KED are calculated at the 20 GHz, 40 GHz, 60 GHz, 80 GHz, and 100 GHz, respectively. In the wide-angle region (i.e., $\arctan(-h/d_2) > 20^\circ$ [16]), where d_2 is less than 2.75 m, the average errors for all the frequencies have the same value of 1.30 dB. However, the average errors for all the frequencies have the same value of 0.04 dB in the narrow-angle region ($d_2 \geq 2.75$ m). Thus, we can find that the key causing the difference between UTD and KED is not the frequency but the angle. Moreover, the characteristics of angles are depicted in Figs. 3(b) and 3(c) directly. The average errors for scenarios 2 and 3 are 1.46 dB and 2.01 dB in the wide-angle region ($|\theta| > 20^\circ$), while they are 0.02 dB and 0.07 dB in the narrow-angle region ($|\theta| \leq 20^\circ$), respectively. The results show that KED is identical to UTD with a low error of less than 0.1 dB in the narrow-angle region, while they have a difference with an error of over 1 dB in the wide-angle region. Furthermore, the average computational time is measured. Both UTD and KED take approximately 8.0 ms for one test. Therefore, simulated results agree with the proposal that, for an absorbing screen, UTD applying the narrow-angle Fresnel approximation is equivalent to KED.

Conclusion: This letter proposed a mathematical derivation to rigorously prove that, for an absorbing screen, UTD applying the narrow-angle Fresnel approximation was equivalent to KED. The simulation scenarios were designed to validate the proposal by comparing KED with UTD in the narrow-angle (less than 20°) and wide-angle (over 20°) regions at mmWave bands (20 GHz - 100 GHz). Simulated results showed that KED was identical to UTD with a low error of less than 0.1 dB in the narrow-angle region, while they had a difference with an error of over 1 dB in the wide-angle region. In addition, the average computational time was measured and resulted in both UTD and KED taking approximately 8.0 ms for one test. Therefore, the simulation agreed with the proposal. From the proposal, it can be theoretically explained the differences and similarities between KED and UTD for an absorbing screen.

Acknowledgment: This paper has been supported by the Commissioned Research through the National Institute of Information and Communications Technology (NICT), Japan, under Grant #02701.

X. Du and J. Takada (*Tokyo Institute of Technology, Tokyo, Japan*)

E-mail: du.x.ab@m.titech.ac.jp

References

1 Rappaport, T. S., MacCartney, G. R., Sun, S., Yan, H., and Deng, S.: Small-scale, local area, and transitional millimeter wave propagation for 5G communications. *IEEE Trans. Antennas Propag.* **65**(12), 6474-6490 (2017)
2 Andrews, J. G., Buzzi, S., Choi, W., Hanly, S. V., Lozano, A., Soong, A. C. K., and Zhang, J. C.: What will 5G be? *IEEE J. Sel. Areas Commun.* **32**(6), 1065-1082 (2014)
3 Rangan, S., Rappaport, T. S., and Erkip, E.: Millimeter-wave cellular wireless networks: potentials and challenges. *Proc. IEEE* **102**(3), 366-385 (2014)
4 Haykin, S. and Moher, M.: *Modern Wireless Communications*. Prentice Hall, Hoboken, NJ, USA (2004)
5 James, G. L.: *Geometrical Theory of Diffraction for Electromagnetic Waves*. IET, UK (1986)
6 Kouyoumjian, R. G. and Pathak, P. H.: A uniform geometrical theory of diffraction for an edge in a perfectly conducting surface. *Proc. IEEE* **62**(11), 1448-1461 (1974)
7 Du, X. and Takada, J.: Design of parameters of fast Fourier transform for three-dimensional split step parabolic equations and mirror Kirchhoff approximation. *IEEE Access* **11**, 44964-44976 (2023)
8 Balanis, C. A.: *Advanced Engineering Electromagnetics*. Wiley, Hoboken, New Jersey, USA, 767-799 (1989)
9 Osipov, A. V. and Tretyakov, S. A.: *Modern Electromagnetic Scattering Theory with Applications*. Wiley, Hoboken, New Jersey, USA, 274-277 (2013)
10 Born, M. and Wolf, E.: *Principles of Optics: Electromagnetic Theory of Propagation, Interference and Diffraction of Light*. Cambridge University Press, UK (2013)
11 Andersen, J. B.: UTD multiple-edge transition zone diffraction. *IEEE Trans. Antennas Propag.* **45**(7), 1093-1097 (1997)
12 Mokhtari, H. and Lazaridis, P.: Comparative study of lateral profile knife-edge diffraction and ray tracing technique using GTD in urban environment. *IEEE Trans. Veh. Technol.* **48**(1), 255-261 (1999)
13 Luebbers, R.: Finite conductivity uniform GTD versus knife edge diffraction in prediction of propagation path loss. *IEEE Trans. Antennas Propag.* **32**(1), 70-76 (1984)
14 Southwell, W. H.: Validity of the Fresnel approximation in the near field. *J. Opt. Soc.*, **71**(1), 7-14 (1981)
15 Du, X. and Takada, J.: Structure of the field behind a dielectric circular cylinder in the lit side of the transition region. *Prog. Electromagn. Res. M* **116**(9), 113-115 (2023)
16 Levy, M.: *Parabolic Equation Methods for Electromagnetic Wave Propagation*. IET, UK, 10-11 (2000)